TB, AK, EJP/196357, 14/07/2005

INSTITUTE OF PHYSICS PUBLISHING EUROPEAN JOURNAL OF PHYSICS

Eur. J. Phys. **26** (2005) 1–16 doi:10.1088/0143-0807/26/0/000

Satellite image eavesdropping: a multidisciplinary science education project

Jean-Michel Friedt

Association Projet Aurore, UFR-ST La Bouloie, 16, route de Gray, 25030 Besançon Cedex, France

E-mail: friedtj@free.fr

Received 11 March 2005, in final form 29 May 2005
Published DD MMM 2005
Online at stacks.iop.org/EJP/26/1

Abstract

Amateur reception of satellite images gathers a wide number of concepts and technologies which makes it attractive as an educational tool. We here introduce the reception of images emitted from NOAA series low-altitude Earth-orbiting satellites. We tackle various issues including the identification and prediction of the pass time of visible satellites, building of the radio-frequency receiver and the antenna after modelling its radiation pattern, and then demodulating the resulting audio signal for finally displaying an image of the Earth as seen from space.

1. Introduction

Low Earth-orbiting weather satellites continuously transmit radio-frequency signals encoding images of the Earth as seen from space. We describe here the successive steps for receiving these images, including

- a presentation of the various kinds of satellites that can be listened at,
- the characteristics of their orbits and the calculation of consequent visibility duration over a given point on Earth (i.e., the time we have to get the image) as well as of the pass dates and times (i.e., when to listen for a given satellite);
- the experimental set-up (the radio-frequency receiver) for listening to such satellites and the modulation schemes in order to understand how to convert the digital data (the demodulated signal received from the satellite) into an image.

Low Earth-orbiting satellites thus transmit images which can be received with a simple and low-cost equipment, accessible to schools and student associations [1, 2].

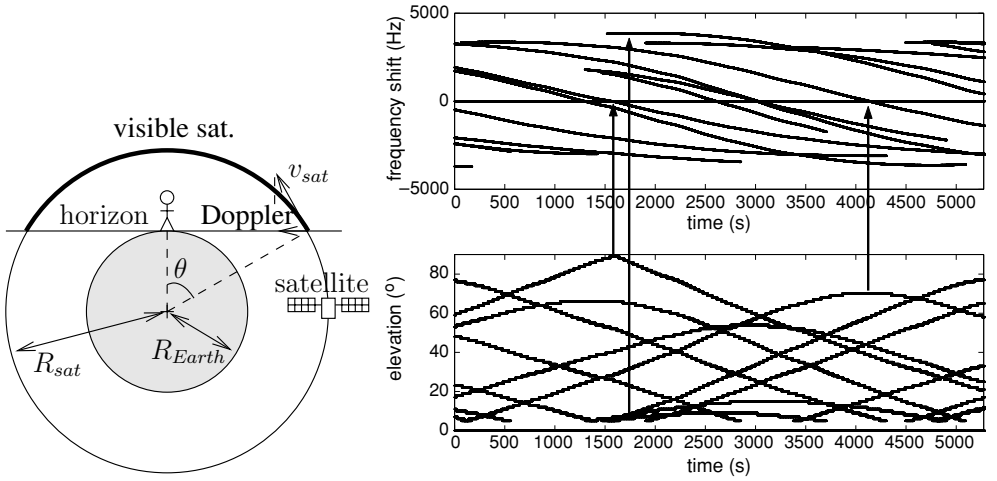

Figure 1. Left: definition of the notations used in the text during the calculations of the orbital parameters of satellites orbiting Earth. Right: Doppler frequency shift observed while receiving signals from satellites of the GPS constellation (measurement performed in Orleans, France, 26 May 2003). The data from several satellites visible at any given time are shown simultaneously. The maximum of the elevation corresponds to a Doppler frequency shift of zero (the radial component of the velocity is null) while this shift is maximum at the horizon (zero elevations).

2. Meteorology satellites

A wide range of satellites orbit Earth, for commercial applications (communications, data or image transmission), military [3–5] (Ikonos [6]) or scientific purposes (Jason, Modis), for amateur radio communications built by AMSAT, [7] or for meteorological observations. We are here mainly interested in this latter set.

We distinguish two main types of weather satellites: those in geostationary orbits (European Meteosats transmitting encrypted data, American GOES satellites openly transmitting data) and those in low polar orbits.

The former orbit Earth at a distance $h_{\text{geo}} \simeq 36\,000$ km from Earth's surface with a period equal to that of Earth's rotation ($T_{\text{geo}} = 23$ h 56 min) [8]. This orbit has been first defined in 1945 by Clarke [9] for keeping a satellite over an approximately fixed point from the surface of our planet [10].

On the other hand, low Earth-orbiting polar satellites are at a much lower altitude of about $h_{\text{polar}} = 800$ km, following a trajectory flying over the poles. They thus quickly pass overhead—following a north–south trajectory. We can estimate the maximum visibility duration of such a satellite from ground by using Kepler's third law [11]: $T^2/R^3 = \text{constant}$ with T the orbit period of a satellite and R the radius of its orbit from the centre of inertia (i.e., the centre of Earth) [12]. Considering that a geostationary satellite orbits Earth at an altitude of about 36 000 km, we deduce the period of a low-altitude polar satellite: $\sqrt{\frac{(R_{\text{Earth}}+h_{\text{polar}})^3}{(R_{\text{Earth}}+h_{\text{geo}})^3} \times T_{\text{geo}}^2} \simeq 101$ min. However, a satellite is only visible when it is over the horizon. Referring to figure 1 in which we illustrate the part $\cos(\theta) = \frac{R_{\text{Earth}}}{h_{\text{polar}}+R_{\text{Earth}}}$ of the orbit observed to be above the horizon from a given point on Earth, we see that only the fraction of the orbit defined by $\frac{2\theta}{2\pi} = 2 \times \arccos\left(\frac{R_{\text{Earth}}}{h_{\text{polar}}+R_{\text{Earth}}}\right)\Big/(2\pi) \simeq 0.151$ is visible from ground, with $R_{\text{Earth}} = 6378$ km Earth's radius [13], hence a maximum pass duration of 15.3 min when the

satellite flies overhead (at zenith), which is indeed the observed value. The same argument shows that the International Space Station, orbiting Earth at an altitude of about 400 km [14], is visible for an even shorter duration: 9.7 min at maximum.

The reception technologies, from the antenna to the receiver and the radio-frequency demodulator, as well as the observation methods (prediction of the pass times of moving satellites) are determined by these differences in the altitude and behaviour (position fixed in space with respect to ground, or moving) [10].

3. Orbits and altitudes: orbital data ('keplers')

3.1. Doppler shift due to satellite motion

We have previously calculated (section 2) the visibility duration of low Earth-orbiting satellites, from which we will deduce the moving speed along the orbit and hence the transmission radio-frequency shift Δf as seen from ground due to the motion of the emitting source through the Doppler effect [15, 16]: $\Delta f/f = v/c$ where f is the emitted frequency in the rest frame of the emitter, v is the velocity of the emitting source along the line of sight and $c \simeq 3 \times 10^8$ m s^{-1} is the velocity of electromagnetic waves in free space. We illustrate this effect with the moving satellites from the Global Positioning System (GPS) constellation which orbit Earth at an altitude of $h_{\mathrm{GPS}} \simeq 20\,000$ km. The same calculation as done previously shows that the orbital period is 707 min (which is close to half a day as required by such an orbit) and the maximum visibility duration is 299 min or about 5 h. These 707 min are used to travel an orbital path of $2\pi(R_{\mathrm{Earth}} + h_{\mathrm{GPS}}) = 166\,000$ km, which leads to a tangential velocity of 3.9 km s^{-1}. Considering now the time at which the satellite crosses the horizon (which is the time at which the Doppler effect is maximum, for later becoming null at the zenith), the orbit is at an angle $\theta = \arccos\left(\frac{R_{\mathrm{Earth}}}{R_{\mathrm{Earth}}+h_{\mathrm{GPS}}}\right) \simeq 76^\circ$ to the horizon and we conclude that the velocity of the satellite towards the ground-based observer is $v_{\mathrm{GPS}} \times \cos(76^\circ) \simeq 0.95$ km s^{-1}. We thus deduce the Doppler frequency shift of the radio signal received f_{observed} from the emitted frequency $f_{\mathrm{GPS}} = 1.5$ GHz: $f_{\mathrm{GPS}} - f_{\mathrm{observed}} = \frac{v_{\mathrm{GPS}}}{c} \times f_{\mathrm{GPS}}$. As a conclusion to this calculation, $(f_{\mathrm{GPS}} - f_{\mathrm{observed}})_{\mathrm{max}} = \frac{v_{\mathrm{GPS}}}{c} \times f_{\mathrm{GPS}} \simeq 4500$ Hz. This value is surprisingly close to that experimentally observed with a Motorola GPS-Oncore VP receiver (figure 1, right) [17][1], considering all the numerical approximations we made during the calculation.

See endnote 1

A similar calculation in the case of the low Earth-orbiting polar satellites of the NOAA series [18, 19] shows that their tangential velocity is 7.5 km s^{-1}, the angle of their orbit when crossing the horizon is $\theta \simeq 20^\circ$ and the maximum Doppler shift is 3050 Hz for a transmission frequency of 137.5 MHz. However, for the modulation scheme of interest here (section 3.3), the frequency modulation of the carrier for transmitting data from the satellite to the ground station avoids Doppler shift related effects. Indeed, the phase locked loop (PLL) used for demodulating the signal is able, under the assumption that its bandwidth is wide enough (which is the case here), to track the frequency of the carrier and the output of the PLL will include an offset to the wanted signal due to the Doppler shift. However, this offset drifts very slowly (related to the speed of the satellite as seen from ground) and will thus be eliminated by the high-pass filters included in the audio demodulation circuit (either on the radio receiver side which eliminates any dc component of the output signal, or on the audio card side). The frequency shift due to the Doppler effect is observed, for example, during amateur radio transmissions around 430 MHz with moving satellites when modulation schemes with much narrower bandwidths are used [20].

[1] The GPS-Oncore VP receiver was bought from Synergy for $35/piece (July 2003 price).

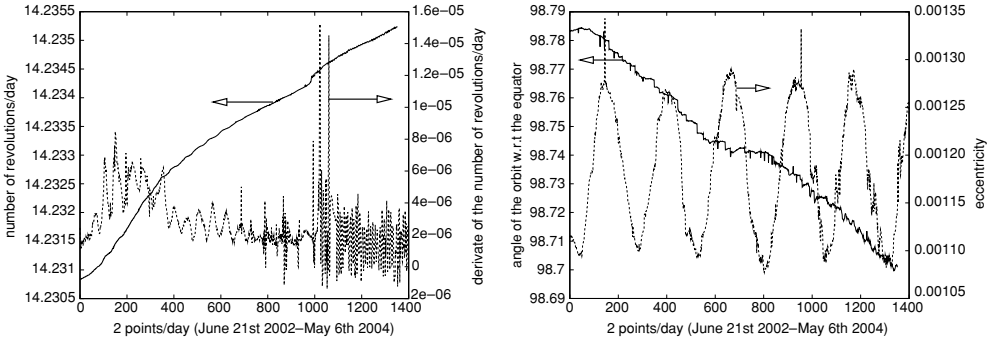

Figure 2. Evolution of the orbital parameters. Left: the number of revolutions around Earth per day—which defines the altitude of the satellite—and its first derivative, for NOAA 17 since it was launched. Right: oscillations of the eccentricity of the orbit, and angle with respect to the plane of the equator [47, 48].

3.2. Prediction of pass schedules

Accurate prediction of the pass schedules of satellites requires the use of models much more sophisticated than the simple classical approximation of a point moving solely under the effect of gravity in vacuum, including friction due to the upper atmosphere. Orbital parameters are distributed following a format due to the American NORAD [21], the agency responsible for following all objects in orbit around Earth (whether satellites, rockets or fragments).

These parameters (two-line elements—TLE) are distributed on Celestrak's web site [22] and are periodically updated. Indeed, even though orbital parameters of geostationary or low Earth-orbiting satellites barely vary over time (and thus only require sparse updates—less than once a month), that is not the case for, e.g., the International Space Station (ISS) whose orbit is often corrected in order to compensate for its fall due to atmospheric drag.

Orbital parameters [23] include the orbit period (figure 2), the angle of the orbit to the plane including the equator, and the eccentricity of the ellipse of which Earth is one of the foci.

For example, a typical two-line element such as

```
NOAA 17
1 27453U 02032A 04141.47085506 .00000028 00000-0 31630-4 0 9103
2 27453 98.7010 214.0435 0012905 114.4615 245.7918 14.23528214 98966
```

indicates that the satellite named NOAA 17 follows an orbit tilted by 98.7010° with respect to the equator (i.e., a polar orbit), with an eccentricity 0.0013 (i.e., a circular orbit) and rotates 14.24 times per day around Earth (in agreement with the previously calculated orbit period of about 100 min). Disturbances due to atmospheric drag are included as first derivative (0.000 000 28) and second derivative (0.0) of the number of daily revolutions in the most simple prediction models, while a drag coefficient in included as the next term (with an additional correction considering the density of the atmosphere at the altitude of the satellite [24]).

Note that the choice of the inclination of the orbit at 98.7° rather than 90° corresponding to a 'truly' polar orbit is dictated by the target of reaching a heliosynchronous orbit. Indeed, this orbit leads to a roughly constant illumination by the sun of every point of Earth when imaged by the satellite. We indeed observe such an effect when monitoring NOAA 17 pass

predictions: this satellite always overflies Besançon (France) around 12:30 (UTC[2]+2), while NOAA 12 and 15 fly over this same location around 1740 h and 1920 h respectively (local summer time), thus providing constant illumination conditions during successive passes.

These orbital parameters are included in orbital models for predicting the pass times and elevations over the horizon of the satellite of interest. We use the Linux-based software Sattrack [26] for predicting the pass schedules.

3.3. Data transmissions

APT mode data transmission [27] is done at a rate of 2 lines per second. Each line includes two images side by side, one obtained at visible wavelengths and the other at thermal infrared wavelengths (around 1.6 μm, wavelength at which the reflectance difference between clouds and snow is most obvious [24]). These images are obtained by rotating a mirror in front of a single optical sensor aboard the satellite following an axis parallel to the trajectory: successive lines of the images are thus continuously transmitted as they are acquired by the sensor and there is no definition of a beginning or an end of a frame as would be expected if the sensor were a two-dimensional picture element (pixel) matrix [24]. The abscissa of a pixel on the received image is thus defined by the rotation angle of the mirror while its ordinate is due to the motion of the satellite. Hence, our image reception capability starts as soon as the radio signal becomes clear—i.e., when the satellite becomes visible over the horizon—and stops when the radio signal disappears. The spatial resolution of images transmitted in APT mode is 4 km/pixel [18], defined by the speed of the satellite—and thus its altitude—and the data transmission speed. Indeed, two successive lines must aim at adjacent regions on the ground. We have seen that the rotation period of a low Earth-orbiting satellite is 94 min during which the satellite scans the 40 000 km of Earth's circumference. Additionally, the satellite transmits two lines every second so the width of a pixel (along the ordinates) must cover the length corresponding to the motion of the satellite during this time span, $40\,000/(94 \times 60) * 0.5 = 3.5\ \text{km} \simeq 4\ \text{km}$. The magnification of the optics aboard the satellite is adjusted so that such a surface is covered when seen from the altitude at which the satellite orbits [24].

Hence, considering that the maximum visibility duration of a satellite is 15 min, that we observe 2 lines per second and that each pixel covers an area of 4×4 km^2, the maximum latitude extension of an image is (since the circumference along a meridian is 40 000 km) $\frac{15\times60\times2\,\text{pixels}\times4\,\text{km/pixel}}{40\,000\,\text{km}} \times 360 = 65^\circ$. Such a span, centred on the longitude of France, extends from the Spitzberg at the north to Mauritania to the south. Such an estimate is positively compared to figure 3, right.

3.4. Modulation schemes

Polar orbiting satellites considered here transmit via carrier frequencies of 137.500 MHz (NOAA 12 and NOAA 15) and 137.620 MHz (NOAA 17) analogue signals which will be captured. The status of polar orbiting satellites (so called POES [28]—Polar Operational Environmental Satellites) is constantly updated on one of NOAA's web sites [29].

The encoding scheme of the signals transmitting the weather images is somewhat complex but very interesting since it provides an opportunity to present several modulation methods (figure 4). We will present here the APT (Automatic Picture Transfer) communication mode used for transmitting analogue data and requiring no complex decoding equipment other than a personal computer with a sound card.

[2] UTC stands for Coordinated Universal Time: local time in different countries is attached to UTC by a whole number of hours [25].

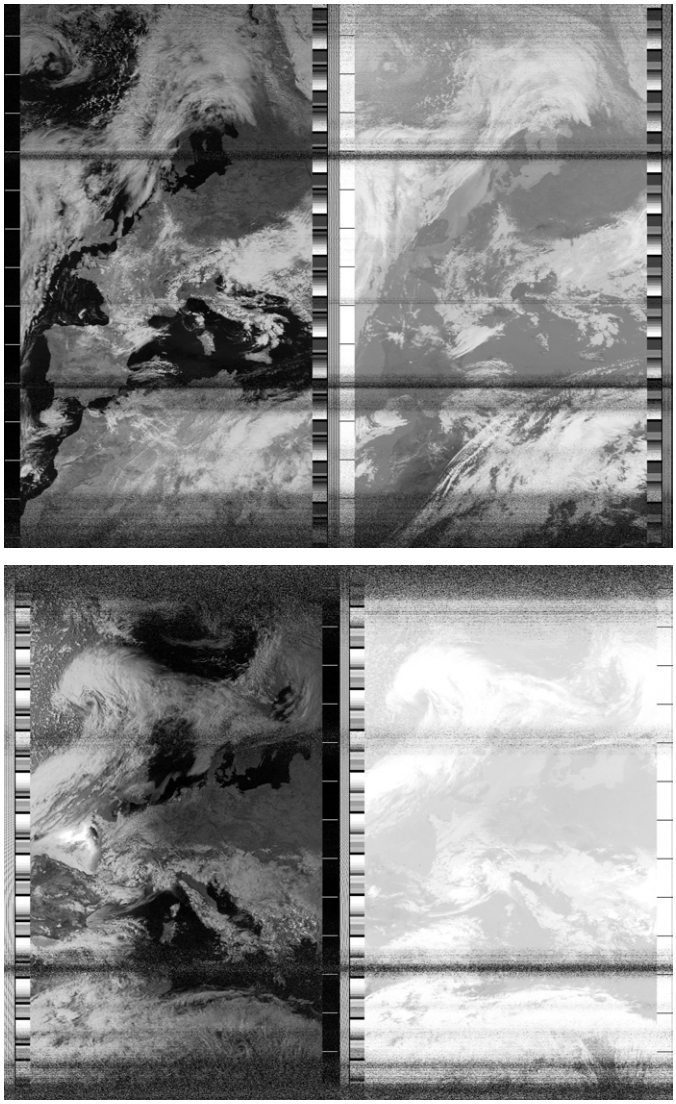

Figure 3. Top: the image emitted by NOAA 17 received on 14 April 2004 at 1224 h local time (maximum elevation: 85.2°). Bottom: the image emitted by NOAA 12 obtained on 14 April 2004 at 1729 h local time (maximum elevation: 81.9°), noticeably aesthetic with the reflection of the sun in the Atlantic ocean. Note the identical spacing of the dark stripes in both images, which we interpret as the position of the nulls of the used antenna (in both cases the crossed dipoles were located at 235 cm from ground).

We start from the signal made of a sequence of pixel values (as obtained by the on-board camera) defined by variable light intensities. These light intensities varying at low frequency modulate the amplitude of a 2400 Hz sine wave. This modulated sine wave itself is used for modulating the frequency of a carrier around 137.5 MHz or 137.62 MHz depending on the satellite.

On the ground, a radio receiver is used in its frequency demodulation mode to convert the radio-frequency signal to an audio signal around 2400 Hz. This signal is recorded by

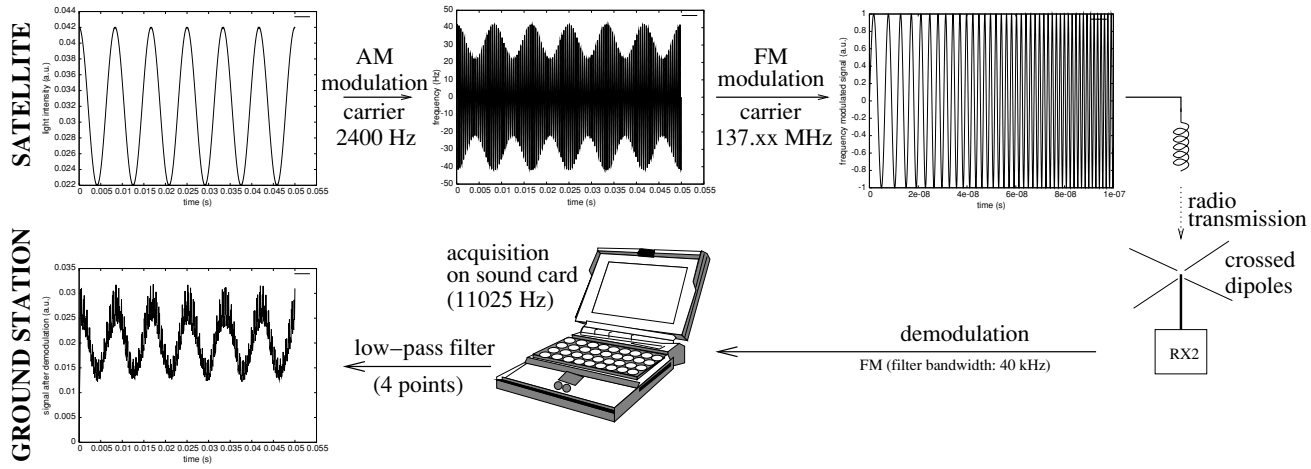

Figure 4. Steps for transmitting pixel values from the satellite to the ground station and results of the demodulation of the AM signals by a band-pass filter (bottom-left). The FM modulation on a 137.xx MHz carrier cannot be depicted on the same time scale: the 2400 Hz sine wave appears as a line on the 100 ns over which the 137 MHz carrier is shown.

the sound card of a computer (sampling frequency: 11 025 Hz, 16 bits/datum in our case), and its amplitude restores the light intensity of each pixel. The easiest way to measure the amplitude of the sine wave is to process it through a low-pass filter with a cutoff frequency below the frequency of the carrier. (Note that averaging several successive samples is the simplest low-pass filter.)

4. Antennas

In the case of the geostationary satellites, the optimal means for getting a good signal-to-noise ratio is to use an antenna with a very high gain[3] and accurately focused in a fixed direction towards the satellite. Such a result is usually achieved with a parabola properly oriented towards the satellite (towards the south in the northern hemisphere since geostationary satellites are located over the equator). The efficiency of this solution increases with the transmission frequency: in the GHz range, the wavelength is smaller than 30 cm. The bigger the parabola, the greater is its gain and the more directional its radiation pattern [31].

Let us remind before any discussion the fundamental relationship used in the field of radio transmissions, relating the frequency f (in MHz) and the wavelength λ (in m) through the speed of light: $\lambda = \frac{300}{f}$. Hence, $\lambda(137.5\ \text{MHz}) \simeq 2.2$ m.

In the case of low Earth-orbiting satellites, transmission takes place in a frequency range easier to access—137.500 or 137.620 MHz—but moving quickly in the sky. The constraints on the selection of the antenna are thus completely different from the previous case. Instead of a highly directional antenna we need an antenna with a radiation pattern as isotropic as possible, without null (direction in space towards which the antenna does not receive any signal), and additionally able to efficiently receive a circularly polarized signal.

Indeed, during data transmission by a radio beam, the polarization of the receiving antenna (defined as the orientation of the electric field to which the antenna is sensitive) must be the same as the polarization [34, p 65] of the emitting antenna. For example, for transmission of television images or amateur radio messages using Yagi antennas commonly visible on roofs, the polarization is horizontal (the dipole [34, p 43] of the Yagi antenna being parallel to ground). However, a satellite is constantly spinning and a linear polarization would appear from ground as slowly rotating. The result would be a periodic loss of signal if the receiver were in a planar polarization. The use of a circular polarization solves this issue: by using an helicoidal antenna or two dipoles phase shifted by 90°, reception not only becomes insensitive to the relative orientation of the emitting and receiving antennas, but also insensitive to possible reflections of the incoming signal (ground, mountains) which might induce a signal loss through destructive interferences (the lack of sensitivity to reflections is a result of the interchange of the hands of circular polarization upon reflection of an electromagnetic wave on a conducting surface while the antenna is built to be sensitive to only one hand of circular polarization).

We apply these somewhat abstract concepts by using a program for simulating the electromagnetic behaviour of metallic structures, NEC [30], available as an updated version under Linux [32]. These simulations will allow us to predict the behaviour of various antenna geometries and to select the most appropriate one.

We have started from the crossed dipole antenna as described at http://www.applet.cz/˜ulcak/crossed_dipoles_ant.htm. The basic idea behind such a design is to combine with a

[3] The gain of an antenna is defined as the maximum increase in signal power transmitted to that which would be emitted if all power supplied to the antenna was radiated isotropically [30]. Hence, antenna gain is related to directivity since the gain increase in a given direction is necessarily obtained by decreasing the power radiated in other directions.

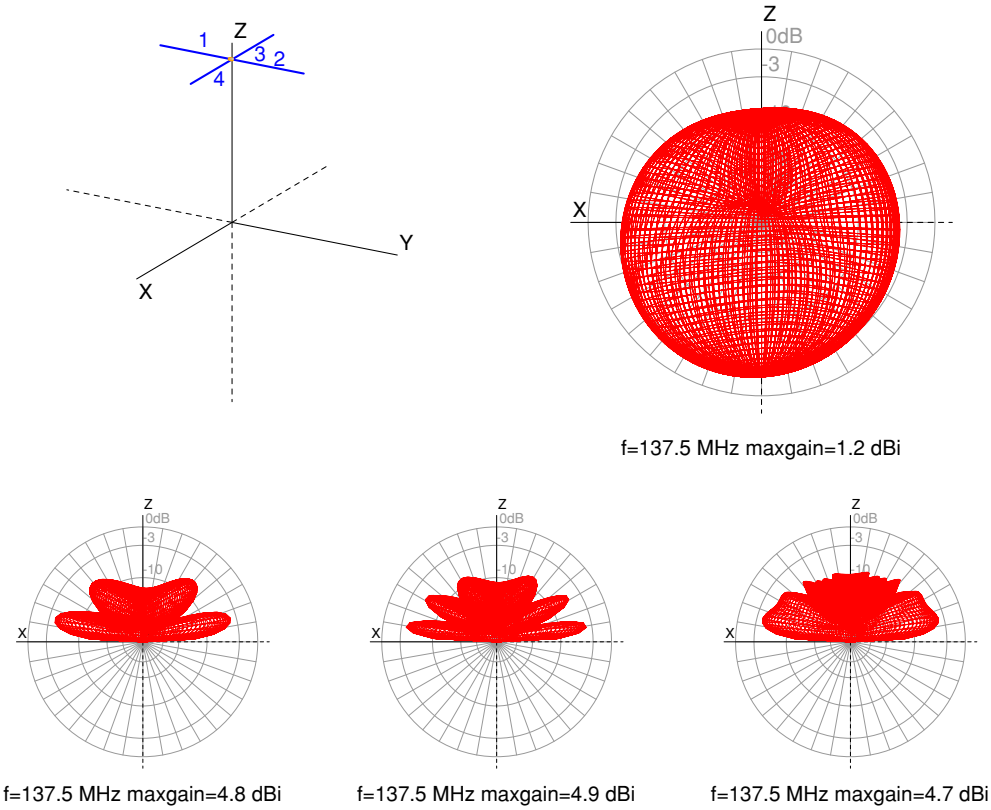

Figure 5. Top: a schematic of the antenna to the left (the pair of crossed dipoles is located here 1.10 m above ground), and the radiation diagram of the antenna in free space (right). Bottom: the radiation diagram as a function of the height of the dipoles over ground. Note the difference with the diagram obtained in free space which would have originally hinted to the aim of isotropic radiation pattern having been achieved with such a geometry. The ground conductivity has been chosen as $\varepsilon_{\rm sol} = 13$ and its conductivity $\sigma = 0.005$ S m^{-1}. From left to right: the dipoles are 2.1 m, 3.1 m and 23.1 m from ground.

(This figure is in colour only in the electronic version)

delay line (a piece of cable of the right length, $\lambda/4$ for a phase shift of 90°), the signals of two orthogonal dipoles. NEC simulations of this circuit show the following:

(i) The two dipoles do not contribute equally and thus the antenna is not isotropic in a plane parallel to ground. This is probably related to different impedances being seen by the two dipoles, the 75 Ω quarter wavelength coaxial cable being certainly not an optimal phase shifter.

(ii) The four reflectors located at the bottom of the antenna are useless and can be removed without affecting fundamentally the radiation pattern. Four beams emanating from the supporting mast are mostly inefficient for providing a proper ground plane [33], and they should either be replaced by a metallic wire-mesh, or with an increased number of beams, or the dipoles should be located above a conducting roof (corrugated iron) which would act as a ground plane.

(iii) A consequence of the previous point is that the radiation pattern is strongly affected by the height above ground at which the crossed dipoles are located. This last point is illustrated in figure 5. The influence of the ground is a fundamental parameter to be included

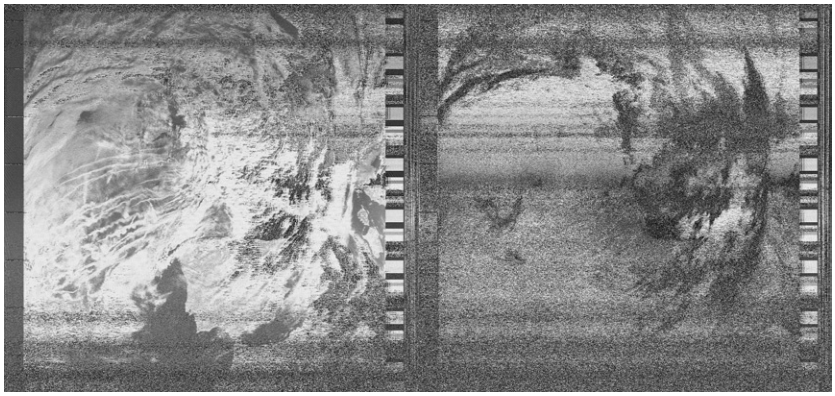

Figure 6. One amongst the best images obtained after two years of receiving satellite images with an AOR3000A wideband radio scanner and a discone Diamond D190 antenna located at the corner of a balcony oriented towards the south-west at the second floor of a four-floor building in Orleans, France (NOAA 17, 01/26/2003). Even though this image is of a good enough quality to get familiar with the technique and identify the shores of western Europe, whites are saturated and the infrared image is of poor quality because of the narrow bandwidth of the IF filter in the NFM mode of the scanner. Note the visibility of tracks due to ships crossing the Atlantic ocean, also visible on the Meteosat image. Compare this image with those of figures 7 and 3.

in modelling the radiation pattern compared to simulations of an antenna in free space (figure 5, top-right) which are practically useless by themselves.

We note in figure 5 the increase of the number of nulls as the antenna rises above ground. More generally, we can consider that N nulls are present when the antenna is at a height of N half-wavelengths above ground [34]. The intuitive solution of positioning the antenna as high as possible is thus not necessarily optimum. We have in our case chosen to locate the dipoles at a height of 235 cm above ground for the images presented here, unless explicitly mentioned otherwise.

5. Radio receivers—demodulation of the resulting signals

Alternately to wideband scanners (figure 6) which only produce poor results, receivers specifically designed for APT image reception are available. We have experimented with the RX2 receiver supplied by the British RIG (Remote Imaging Group [35]) as a kit.

Once the radio signal is demodulated, the resulting audio-frequency signal is digitalized using the sound card of a personal computer for further processing, either with a software available for free but only in binary format—`wxtoimg` [36] for Linux, Windows and MacOS—or by processing with Matlab/octave. Indeed, we know that the 2400 Hz audio signal is amplitude modulated with the amplitude of the signal being representative of the light intensity of the final image. Considering that the audio signal was sampled at a rate of 11 025 samples per second, we know that one period of the carrier fits in 4 or 5 samples ($11\,025/2400 \simeq 4.6$) and we can thus take the greatest of the absolute values of any four successive points in order to get an estimate of the amplitude of the carrier during this period. The list of resulting data is reshaped to a matrix format as a series of lines including as many pixels as the sampling frequency divided by the number of points over which the average was taken, divided by 2 (since two lines are transmitted every second).

The software `wxtoimg` is more powerful since it phase-locks the audio signal demodulation on the AM carrier (assumed to be at 2400 Hz) and identifies the beginning of each line in order to compensate for any difference between the remote oscillator aboard the satellite and the local oscillator available on the sound card. Furthermore, this software is also able to predict the satellite pass schedule (and hence check the dates and times obtained with `sattrack`) as well as in the most up to date version at the time of writing (>2.5.7), to overlap a map of the borders of the countries visible on the raw image. A comparison of the results obtained with the professional software and with our much simpler algorithm is presented in figure 7.

We can, however, gather a useful information from the shape of the image (figure 7, left) obtained by our simple demodulation scheme. We observe that the resulting 1379×1784 pixels image displays a drift from top to bottom of 263 pixels (as measured on the central calibration band). We know that 1379 pixels in abscissa represent 0.5 s and that the 1798 lines in ordinate lasted 892 s of listening time. The drift over the duration of this acquisition is thus $263 \times 0.5/1379 = 0.095$ s, or $0.095/892 = 106$ ppm. We attribute this error to a drift of the reference oscillator, 100 ppm being typically the order of magnitude of the frequency stability of those TTL oscillators sold for low-cost computer applications (see, for example, the specifications of the C-MAC oscillators, referenced by the manufacturer as IQXO-36 [37]). Much better results are expected by replacing the sound card oscillator with a temperature controlled oscillator or by locking this oscillator on the GPS' 1 PPS signal.

6. Some digital image processing

An image processing function available in `wxtoimg` which we often use to improve the contrast of the images presented in this document is *histogram equalize*. We will present here this algorithm, after emphasizing the fact that this algorithm is only a signal processing tool and has no physical meaning if an additional quantitative processing of the satellite images is to be performed (for example, extracting temperatures from infrared data), and its purpose lies only in the aesthetic rendering of the data [24, 38].

A greyscale image is characterized by a histogram of colours, defined as the number of pixels of a given shade normalized by the total number of pixels. This distribution can be considered as the probability of finding in the image a pixel of a given shade. The wider the range of colours over which the histogram is spread, the better the contrast of the image. Hence, a histogram characterized by a sharp peak, localized, is characteristic of an image with most pixels of the same colour. In contrast, a uniform histogram (constant over the colour range) characterizes a well-contrasted image in which all the colours are present in equal proportions. This latter result is the one we aim to obtain, as shown in figure 8.

Rather than discussing in terms of the histogram $h(c)$ being the distribution of the greyscales c, we will consider the cumulative histogram $H(c)$ which is deduced from the greyscale histogram $h(c)$ by $H(c) = \sum_{n=0}^{c} h(n)$: the value of the cumulative histogram at abscissa c is given by the sum of all the values of the histogram to this point. Since the histogram includes probabilities and hence positive values, $H(c)$ is a function increasing with c. Furthermore, we easily show that the cumulative histogram of a constant histogram is the line of slope 1, going through the origin, if we define the range of colours in the interval $c \in [0; 1]$. The problem thus comes down to finding a translation of the colours c in the interval $[0; 1]$ towards $[0; 1]$ which converts the experimental cumulative histogram $H(c)$ into a new cumulative histogram described by the line of slope one running through the origin.

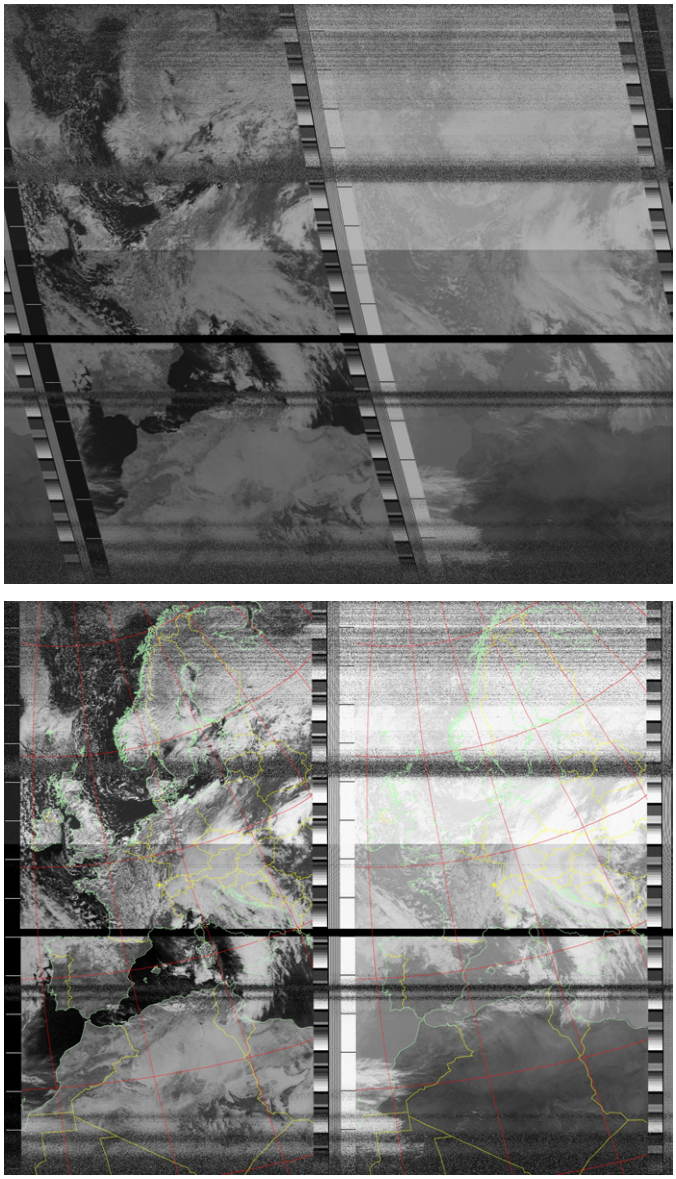

Figure 7. Top image: the demodulation result of a NOAA 17 signal obtained on 23 March 2004 (1224 h local time, maximum elevation: 84.7°) using `octave` under Linux by averaging the sound data (11 025 Hz, 16 bits/sample) over four successive points. Although this algorithm works under Matlab, the latter was unable to complete the full calculation on the same computer (400 MHz Intel CPU, 128 MB RAM) running under Windows98, probably because of the poor memory management by this operating system. Bottom: the demodulation result by `wxtoimg`. Note that this professional software also provides the ability to overlay the borders of the observed countries. The left-half of each image is obtained in the visible wavelengths while the right is in the infrared range. The black stripe around the French–Spanish border is due to a manipulation error on the sound level during the recording.

The solution to this problem is simply to convert the original abscissa axis c into a new axis $H(c)$: the original graph $c \rightarrow H(c)$ is then converted to $H(c) \rightarrow H(c)$ which is

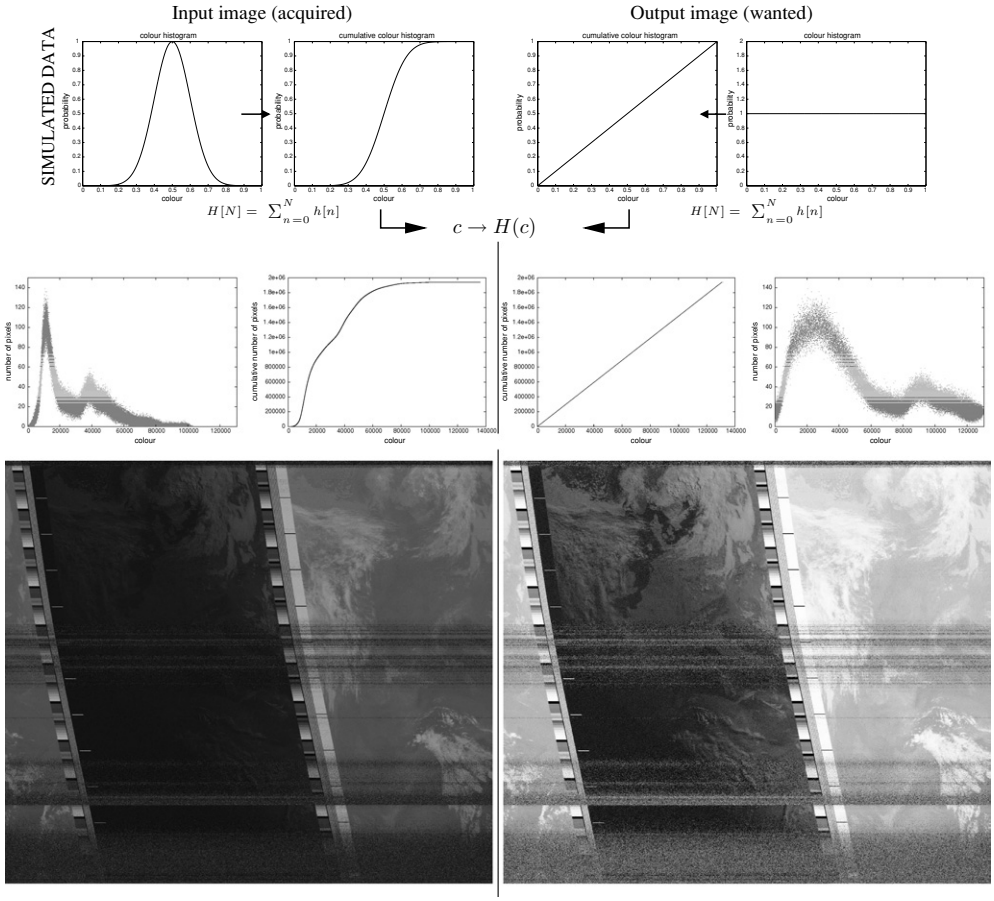

Figure 8. Top: simulation of the evolution of the colour histograms and cumulative histograms of the input images (left) and output after processing (right), with the aim to transform a random pixel distribution to a flat histogram. We see here that the transformation to be applied for converting the input histogram to a cumulative histogram characterized by a line of slope 1 running through the origin is the function $H(c)$ to the input colours c, where $H(c)$ is the cumulative histogram of the input image. Centre: the same graph, but for the images presented at the bottom. Bottom: a raw image to the left (obtained from NOAA 12, 8 June 2004 at 0656 h local time from Besançon, France, with a maximum elevation: 82.5°) resulting from the application of the Matlab script presented previously, and after histogram equalization processing to the right. Note that after processing the appearance of the shores is still in darkness.

indeed the line of slope 1 we were looking for. We thus find back the theorem [39] claiming that

if H is the cumulative histogram of the values of the pixels of the input image, then applying the function H to the input image leads to a resulting image with a constant colour histogram. Practically, this function is available under Matlab (Image Processing Toolbox) and octave under the name `histeq()`.

An extension of this technique is the histogram specification $c \rightarrow G^{-1}(H(c))$ with G the cumulative histogram to be obtained after processing (the case demonstrated previously is $G = Id$).

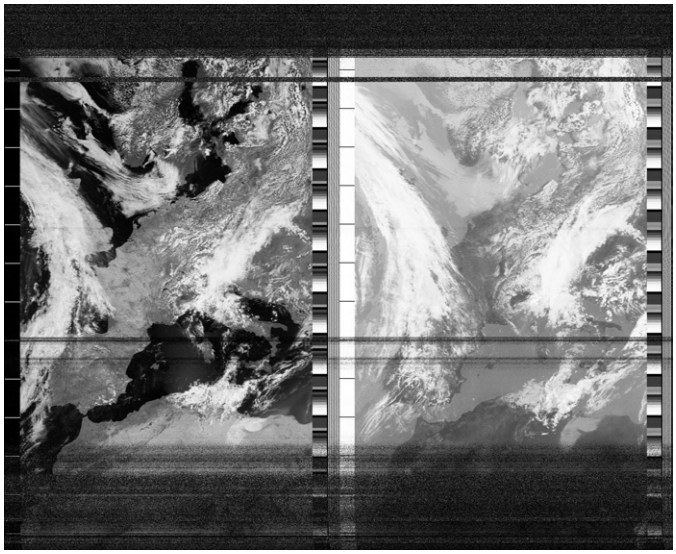

Figure 9. The image obtained on 28 May 2004 at 1224 h (local time) from Besançon (France) during a pass with a maximum elevation of 84.4°. Note the contrail tracks left by planes flying over the south-west of Spain, visible in the infrared image but not in the visible one. The dipoles of the antenna were here exceptionally located at a height of 135 cm from ground, leading to the absence of horizontal bands due to signal loss at the latitude of France as seen in the other images (figure 3).

7. Results

The first satisfaction is to be able to display images gathered from a satellite while it is flying over the receiving station. We provide two image examples (figure 3) obtained from Besançon (France, GPS coordinates: 47.230N, 6.030E) using a crossed dipole antenna and a RX2 receiver.

Beyond the aesthetic aspect, several analyses can be performed on these images:

- Using the behaviour of the satellite as a moving radio source with a perfectly well-known elevation. We use this source to analyse whether the models of the antenna we built are appropriate, and eventually to deduce what modifications to bring to improve the images we obtain (the parameter easiest to tune in our case is the height of the dipoles above ground—235 cm for the images shown in this document). One can compare the images (figures 3 and 9) to illustrate this effect: the banding on these images is attributed to the nulls in the antenna diagram which match well the null directions predicted by numerical simulation as shown in figure 5, bottom-left. Although limited to a single frequency (137.xx MHz) and a single polarization type, using low Earth-orbiting satellites as moving radio-frequency emitters whose coordinates are well known from orbit prediction provides an excellent solution to the otherwise difficult problem of experimental antenna radiation pattern drawing. **See endnote 2**
- Weather forecasting and matching visual and temperature observations (as seen in the infrared images), analysing the complementarity of the information extracted (the two methods observe clouds at different altitudes and the cloud-forming following different mechanisms, such as, for example, contrails [40] which are visible in the IR and not in the visible range: figure 9 to the south-west of Spain. As opposed to the tracks which are due to low-altitude fog condensed from particles coming from the engine exhausts of ships **See endnote 3**

visible over the Atlantic ocean in figure 6 (right image), contrails (*condensation trails*) are cold, high-altitude crystallized clouds). The increase of cloud coverage by contrails due to human activity has been proposed as a possible source of climatic changes [41]. This same principle is used in space exploration in which various wavelengths are used to probe various cloud heights formed by the condensation of different gases [42, 43].

- Applying image processing methods to improve the contrast (definition of the greyscale histograms is required to enhance various properties of the images), identification of the seashores or characteristic cloud structures (vortices). Weather images obtained here provide an invaluable source of data for developing various types of signal processing techniques, including digital phase-locked loops on the audio signal for detecting the start of each new line and synchronizing the local oscillator to the emission rate of the images as defined on the satellite. We have illustrated a basic image processing technique for improving the contrast of the resulting image, which can be considered as a preliminary step towards pattern identification and cross-correlating features observed in the two images observed in the visible and infrared wavelength ranges.
- From a geography point of view, identifying significant areas as seen from space (Neuchâtel, Léman and Constance lakes, urban area around Paris and Seine river, snow-covered Alps in winter for example; figure 9). Under the best circumstances, for images acquired a few hours before sunset, the reflection of the sun in the Atlantic ocean combined with the projected shadow of the clouds illuminated at a grazing angle provides exceptional images (figure 3, right).

8. Conclusion and perspectives

We have presented the reception of satellite images as a multidisciplinary educational project, providing the opportunity to apply a wide diversity of science subjects, either technological with the realization of the radio receiver and of the antenna, or theoretical with the analysis of the orbits or the data transmission and modulation schemes [44, 45]. The applied fields range from physics with celestial mechanics and electromagnetism required for antenna modelling, to programming for data demodulation and processing via electronics and geography with the identification of noticeable regions on ground.

The obvious sequel to this study would be the installation of a small parabola and the realization of the electronics required for receiving images from geostationary GOES satellites. Another aspect of studying satellites is to complement radio signal reception with visual observations, since many bodies in orbit around Earth become visible a few hours after dusk or before dawn, thanks to the reflection of the Sun on the solar panels or on transmission antenna [46].

Finally, bear in mind that those same satellites include onboard sensors other than those providing optical images, including cosmic particle detectors and magnetometers. Those data are available nearly in real time on the web at http://sec.noaa.gov/Data/.

The latest of the series of low Earth-orbiting polar satellites, NOAA-N, has been successfully launched on 20 May 2005 and has been renamed NOAA-18, transmitting APT images at 137.9125 MHz [49].

Acknowledgments

We thank F Vernotte, director of the Besançon Observatory, for kindly hosting the student association Projet Aurore. F Tronel (F1SDZ) proposed the use of NEC for simulating radiation patterns of antennas.

References

[1] Summers J 1989 *Educator's Guide for Building and Operating Environmental Satellite Receiving Stations—NOAA Technical Report* NESDIS 44, US Department of Commerce, National Oceanic and Atmospheric Administration (http://npoesslib.ipo.noaa.gov/techlib/doc41/doc41.pdf)
[2] Reynolds R 2003 Using weather satellites in physics education *Eur. J. Phys.* **24** S83–S97
[3] Bamford J 1983 *The Puzzle Palace* (London: Penguin Books) p 242
[4] Bamford J 2002 *Body of Secrets* (New York: Anchor Books) p 466
[5] Wheelon A D 1997 Corona: the first reconnaissance satellites *Phys. Today* **50** 21–30
[6] http://www.spaceimaging.com/
[7] http://www.amsat.org/amsat/AmsatHome.html
[8] Halliday D and Resnick R 1978 *Physics, Parts 1 and 2* 3rd edn (New York: Wiley) p 366
[9] Kelso T S 1998 *Basics of the Geostationary Orbit, Satellite Times* http://www.celestrak.com/columns/v04n07/
[10] Chalmers J S 1987 Ground trajectories of geosynchronous satellites and the analemma *Am. J. Phys.* **55** 548–52
[11] Tan A and Cameides W L 1981 Kepler's third law *Am. J. Phys.* **49** 691–2
[12] Edge R D 1985 Distinction between center of mass and center of gravity—oscillation of rod-shaped satellite as an example *Am. J. Phys.* **53** 1002–4
[13] http://nssdc.gsfc.nasa.gov/planetary/factsheet/earthfact.html
[14] http://www.hq.nasa.gov/osf/station/viewing/issvis.html
[15] Bensky T J and Frey S E 2001 Computer sound card assisted measurements of the acoustic doppler effect for accelerated and unaccelerated sound sources *Am. J. Phys.* **69** 1231–6
[16] Cook G and Lesoing T 1991 A simple derivation of the doppler effect for sound *Am. J. Phys.* **59** 218–20
[17] Motorola 1998 *Oncore User's guide, Rev. 3.2* http://www.synergy-gps.com/TR_Manual.html
[18] NOAA-L (NASA and NOAA), poes.gsfc.nasa.gov/history/noaal/noaal.pdf
[19] NASA and NOAA 2000 *NOAA-L Press kit* www.gsfc.nasa.gov/gsfc/earth/noaal/noaa-l_presskit.pdf
[20] http://www.qsl.net/vk3jed/doppler.html
[21] http://www.norad.mil
[22] http://celestrak.com/NORAD/documentation/tle-fmt.shtml
[23] http://artemmis.univ-mrs.fr/cybermeca/Formcont/mecaspa/CODE_TLE/CODE_TLE.HTM
[24] Rees W G 1990 *Physical Principles of Remote Sensing* (Cambridge: Cambridge University Press) pp 97–8, 104, 188, 196
[25] Audoin C and Guinot B 2001 *The Measurement of Time—Time, Frequency and the Atomic Clock* (Cambridge: Cambridge University Press) p 257
[26] http://packages.debian.org/stable/hamradio/sattrack
[27] Goodrum G, Kidwell K B and Winston W 2000 *NOAA KLM User's Guide* US Department of Commerce, National Oceanic and Atmospheric Administration http://www2.ncdc.noaa.gov/docs/klm/html/c4/sec4-2.htm
[28] http://poes.gsfc.nasa.gov
[29] http://noaasis.noaa.gov/NOAASIS/ml/status.html
[30] ARRL Antenna Handbook 1997 pp 2–12
[31] Mudgway D J 2001 *Uplink-Downlink. A History of the Deep Space Network 1957–1997* (NASA) history.nasa.gov/SP-4227/Uplink-Downlink.pdf
[32] http://www.nec2.org
[33] http://www.cebik.com/vdgp.html
[34] Balanis C A 1997 *Antenna Theory, Analysis and Design* 2nd edn (New York: Wiley) pp 127, 169
[35] http://www.rig.org.uk
[36] http://www.wxtoimg.com/
[37] http://www.cmac.com/mt/databook/oscillators/leaded/spxo/siqxo_35.html
[38] Pearson H 2005 CSI: cell biology *Nature* **434** 952
[39] http://www.dai.ed.ac.uk/HIPR2/histeq.htm
[40] http://www.epa.gov/otaq/regs/nonroad/aviation/contrails.pdf
[41] Travis D J, Carleton A M and Lauritsen R G 2002 Contrails reduce daily temperature range *Nature* **418** 601
[42] Miner E D and Wessen R R 2001 *Neptune. The Planet, Rings and Satellites* (New York: Springer-Praxis) p 89
[43] Harland D M 2000 *Jupiter Odyssey. The Story of NASA's Galileo Mission* (New York: Springer-Praxis) pp 251, 255, 264
[44] home.fnal.gov/ prebys/talks/satellite_seminar.pdf
[45] http://www.hep.princeton.edu/marlow/satlab/
[46] Kelso T S 1996 *Visually Observing Earth Satellites, Satellite Times* http://www.celestrak.com/columns/v03n01/
[47] Farina C and Tort A 1988 A simple way of evaluating the speed of precession of orbits *Am. J. Phys.* **56** 761–3
[48] Jiang H X and Lin J Y 1985 Precession of Kepler's orbit *Am. J. Phys.* **53** 694–5
[49] http://www.mike-rupprecht.de/afu/index.html?sat/wetter/sat_noaa18.html

Endnotes

(1) Author: Please check the sense in sentence ‘We thus deduce the Doppler frequency shift of the radio signal received . . . ’ after a minor grammatical change made to it.
(2) Author: Please check the numerical value in expression ‘137.xx MHz’ here and elsewhere.
(3) Author: Please check the sense in sentence ‘two methods observe clouds at different altitudes and cloud-forming following different mechanisms . . . ’ after the change.